Bar-Ilan - YeshivaUniversity

Summer Science Research Internship Program 2018

INTRODUCTION

The Bar-Ilan University-Yeshiva University Summer Science Research Internship Program is an amazing research opportunity for undergraduate men and women, allowing them to contribute to the forefront of science research taking place in Israel. Generously supported by former chairman of Bar- Ilan's Global Board of Trustees, Dr. Mordecai D. Katz, and his wife Dr. Monique Katz, and by the J. Samuel Harwit, zt"l & Manya Harwit Aviv Charitable Trust, students gain invaluable laboratory skills, along with an unforgettable summer experience.

Program Director: Prof. Arlene Gordon
Av and Em Bayit: Rav Chaim and Ronit Goldberg

Table of Contents

Editors-in-Chief: Anna Schuman and Binyamin Kaplan

Engineering

(L-R) Elisheva Muskat, Nitzana Jessica Penn, Bezalel Pittinsky, Yehuda Goldfeder, Binyamin Kaplan, Zvi Goldstein

Remote Sensing of Brillouin Scattering in Optical Fibers

Zvi Goldstein
Advised under Prof. Zeev Zalevsky and PhD students Sagie Asraf and Nisan Ozana

As more and more structures are built in our ever-progressing society, from buildings and bridges to aircraft, there has been a growing need for methods that can accurately measure wear and tear in order for preventive action to be taken before structural failure occurs. One possible phenomenon that can be exploited to this end is the direct correlation between the strain in an optical fiber and the Brillouin frequency shift.

All matter which has a temperature above 0 Kelvin vibrates, although it may not be perceptible to humans. The Brillouin frequency of an optical fiber is equal to the natural frequency at which the optical fiber vibrates, assuming there are no external factors. However, environmental stresses, such as strain and temperature, can cause the Brillouin frequency of the fiber to shift. This change in frequency is called the Brillouin frequency shift (BFS).

My research this summer was focused on testing the ability of a new imaging technique, called secondary speckle pattern imaging (SSPI), to measure the BFS of an optical fiber remotely. SSPI is performed using a laser and a high-speed camera. The laser is directed at the object of interest. Because of the microscopic roughness of the object, the light that is reflected off the object is deflected in all directions, causing the dispersed light to interfere with itself. The camera captures the back-reflected light as a speckle pattern, with the lighter patches demonstrating constructive interference, and the darker patches demonstrating

destructive interference. Incredibly, movement of the object while the SSPI is running causes the speckle pattern not to change, but to shift. This shift in the speckle pattern occurs in a manner which is proportional to the movement undergone by the object. As such, by using correlation software, the vibration frequency of the fiber can be reproduced from the cyclic shifting of the speckle pattern.

The hope is that by using the technique of SSPI, optical fibers alone can be installed on a structure and used to quantify the various strains affecting the structure, bypassing the wiring and equipment that would be needed if the BFS were to be obtained by performing spectroscopy on the back reflected light from inside the optical fiber.

Integrating Sphere: Using Spectroscopy to Find Optical Properties

Nitzana Jessica Penn
Advised under Dr. Dror Fixler and PhD Student Inbar Yariv

Optical Properties, like absorption, scattering and reflectance of cells are important in detecting diseased cells. Healthy cells have certain known and tested optical properties. In a diseased cell, like a cancer cell, these optical properties will change. To observe these differences, optical set-ups are made and used to test samples.

I created a new optical set-up in Professor Fixler's lab that is centered around an integrating sphere. An integrating sphere, shown in Figure 1, is a hollow sphere whose interior is covered with a white reflective coating causing most of the light to be reflected inside the sphere. There are 4 open ports on the sphere, used for the light source, detector, samples. We can use the ports freely, and close up the ports that are not being used. We used a white light source attached to one of the ports and an Avantes spectrometer, as our detector, attached to the port 90° from the light source. To measure reflectance or absorption of a sample, we put the sample on another port, closed up the fourth port and took measurements. To measure transmittance, we put the sample on top of the light source and closed up the other two ports while measuring. Other types of measurements can be obtained by changing the use of the ports on the sphere.

Figure 1: Integrating Sphere

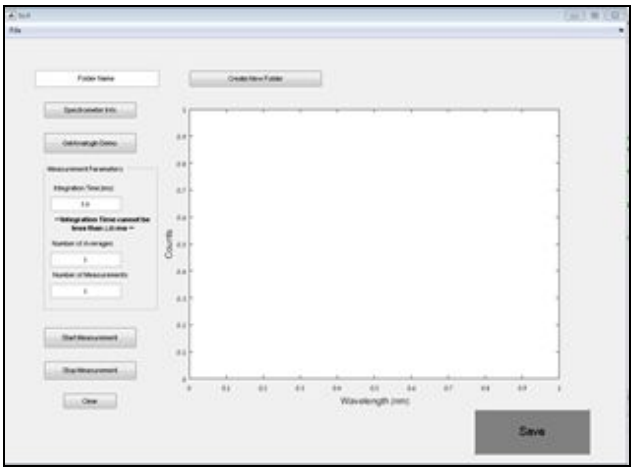

Figure 2: Matlab GUI

In addition to the physical set-up, I created a GUI, or Graphical User Interface, on Matlab. I connected the GUI to the spectrometer so that it is able to control the measurements and show the output. The GUI, as shown in Figure 2, lets the user choose the parameters for measuring like integration time, the number of scans to average and the number of measurements to take per scan. After choosing parameters, the user presses "Start

Measurement" and the output will appear on the graph. After obtaining the data, the user can then save it to an excel file.

When anyone wants to use the integrating sphere, they can change the set-up to whatever they need and then use the GUI for obtaining the data. This will be done by people in the lab who want to know the optical properties of any sample.

Use of Data-Structures for the Design of Hardware Components

Binyamin Kaplan
Advised under Dr. Adam Teman and Hanan Marinberg

When designing complex chips, engineers are faced with difficulties in properly organizing and maintaining the many electrical connections inside the silicon wafer. Various hardware descriptive languages (HDL) exist for the design and manufacture of computer chips. However, these languages, such as TCL and Verilog, are far too cryptic for an engineer to read and manipulate while making changes to a design. In the Emerging Nano-scaled Integrated Circuits and Systems (ENICS) laboratory, a software tool, codenamed Salamandra, was developed to aid in the design of complex computer chips.

Many issues arise when working in the field of chip design, in particular when dealing in Very Large Scale Integration (VLSI) which may employ millions or billions on transistors on a single die. For example, large parts of a chip may work synchronously on the same clock, but may become out of step because of small pathlength differences between the oscillator crystal and the various components that it reaches. Because of this issue, parallel operations may take place in series, or possibly out of order, causing race conditions that may cripple an entire system.

One major drawback to current software packages is their limited, or lack of, Guided Place-and-Route functionality. After designing the logical connections and systems within a chip, the underlying transistor layout must be placed onto a silicon wafer for manufacturing at a semiconductor manufacturer. This process is primarily done by complex algorithms when dealing with larger layouts. However, a designer may choose to use Guided Place-and-Route for subsystems within a chip to create a more efficient and reliable system. Guided Place-and-Route allows the designer to instruct the algorithm about the relative positions of various devices. For example, a Place-and-Route algorithm may separate the various cells of a RAM device on the wafer, and further separate the device from its other connections. Using Guided Place-and-Route enables the engineer to keep components closer together, improving reliability and space efficiency.

Salamandra was built in Python from the ground up to allow for easy designs and more effective placement algorithms. Because it is built on a standard cell library, Salamandra is constantly being expanded with new devices built from existing software components. My work involved writing programs that allowed an engineer to easily transfer TCL and Verilog code into the Salamandra library. The research I performed will enable designers to create more efficient chips faster, by having easy access to the full device library of large semiconductor manufacturers.

Application of Model Verification and Synthesis to Biology

Yehuda Goldfeder
Advised under Dr. Hillel Kugler

Formal Verification is a growing field that has seen major successes in the verification of critical software and hardware systems. It is commonly used in such diverse areas as nuclear power plant safety, airplane engine control, and hardware chip design. Modern techniques can analyze massive state-spaces while avoiding exponential state explosion by using a symbolic representation of the system.

Accordingly, verification tools are promising as a means to analyze complex biological systems which also suffer from the same state explosion problem. One problem of interest is the analysis of gene interaction within cells. While experimental data can provide the state of various genes at different time points, the actual interactions that led from one state to the other remains a mystery.

Verification can help solve this mystery. The Reasoning Engine for Interaction Networks (RE:IN) has been developed for this purpose[1]. It reads in an encoding of the biological system as an Abstract Boolean Network (ABN), where critical components (genes) as well as interactions, both known to exist and merely possible, can be specified. Each component can have a list of possible activation functions. The experimental data, consisting of known states of the system at various time points, is read in as well. It then uses the Z3 SMT solver to identify which concrete networks are consistent with the data and if any interactions or activation functions are required or disallowed.

[1] Boyan Yordanov, Sara-Jane Dunn, Hillel Kugler, Austin Smith, Graziano Martello, Stephen Emmott. A method to identify and analyze biological programs through automated reasoning, npj Systems Biology and Applications, 2016, Volume 2

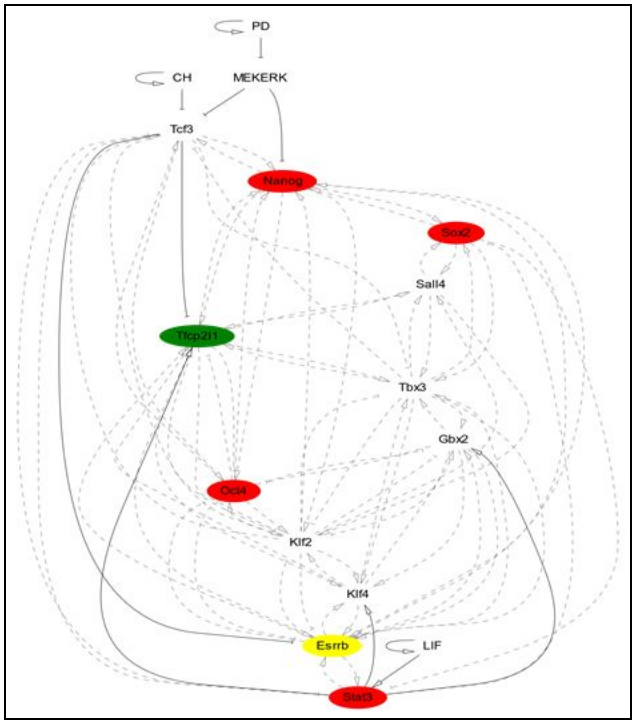

Figure 1: An ABN with uncertain interactions represented as dotted lines

The Network Analysis Engine (NAE) is an ongoing project intended as an alternative to RE:IN. It reads the same model and observation files, but instead performs verification by creating a model in NuSMV, a symbolic model verification language. The experimental data is expressed using temporal logic. The project's long term goals are to support a wider feature set than RE:IN, based on the greater expressiveness of NuSMV, as well as to try to find optimizations to allow the analysis of larger networks.

NAE has multiple modes that can encode the ABN and perform verification in different ways. Some modes represent the experiments using Computation Tree Logic (CTL) and verify them using Binary Decision Diagrams (BDDs) while other modes express the experiments using Linear Temporal Logic (LTL), and verify them using bounded model checking with a SAT solver. A limitation of LTL is that it can only quantify specifications on linear paths and cannot look at distinct branches. This posed a problem, as often

models are analyzed based on multiple experiments that cannot all be satisfied at once but can be satisfied from a single concrete model based on different paths it could take. To get around this, NAE has two solutions. One mode encodes the experiments linearly, and the LTL quantifies a path that solves all experiments, and another mode encodes the experiments in parallel using redundant variables, and the LTL expression addresses all experiments at once.

The results were promising. Using these techniques, NAE was able to solve for concrete networks in large models containing 16 components with multiple activation functions and over 80 interactions, the majority of which were optional, doing so in a time frame comparable to RE:IN, often finding an initial solution much sooner. In general, the CTL mode performed better on smaller models, the parallel LTL mode was best on large asynchronous models, and both LTL modes performed well on large synchronous models, with the parallel mode being superior when many experiments were being considered.

Gain Cell Memory

Bezalel Pittinsky
Advised under Dr. Adam Teman, Roman Golman and Robert Giterman

The Enics lab at Bar Ilan has developed a new kind of embedded DRAM with performance characteristics in between that of SRAM and traditional DRAM. This new DRAM, called Gain-Cell memory, stores a bit in the parasitic capacitance between two transistors. Unlike traditional DRAM, Gain-Cell memory can be manufactured in the typical MOSFET fabrication process. This allows it to be placed on the same die as the processor, enhancing speed and compactness, ideal for mobile devices where one wants as many components possible on the SoC. Such DRAM which can be embedded on the cpu die is known as embedded DRAM (eDRAM). It is theorized that this new memory will consume less power than both SRAM and conventional DRAM, making it all the more attractive for use in mobile devices. Gain-cell memory is 3 or 4 transistors per cell, making it bigger than DRAM but smaller than SRAM. Unlike conventional DRAM, gain-cell memory doesn't lose its contents when it is read. This allows for less clock cycles and power wasted refreshing the memory, further enhancing speed and power-efficiency. This speed is only further increased by the gain-cell memory's proximity to the processor. Although not as fast as SRAM, gain-cell memory is thought to be far faster than conventional DRAM, making it potentially useful as high level cache.

The lab has designed a chip called BEER to test the gain-cell memory to see under what conditions (voltages, clock speed, retention time) it works best. The chip itself contains arrays of 4 transistor and 3 transistor gain-cell bits, controlling logic known as BIST, and an array of SRAM as control to test the gain-cell arrays against. The BEER chip is placed in a custom PCB with many sockets for power supplies, allowing for full control of all voltages in the chip. The PCB is attached to an FPGA that sends BEER data and instructions for how to deal with the data. The FPGA and power supplies are controlled by a Perl script running on an ordinary PC. This Perl script sends FPGA instructions to the FPGA and sets voltages, div_factor, and DCO (the latter two are parameters to change the clock speed) of BEER. The FPGA code is generated by a matlab script which can be tweaked to send different patterns (1s vs 0s), retention time (how long BEER waits before reading a bit), size of test array, and various

configuration parameters for the sense-amplifiers. Retention time is important for determining how long a bit can go without needing to be refreshed. The sense-amplifiers amplify the signal (1 or 0) from a bit after it is read. On the memory array there are two kinds of sense-amplifiers and it had to be determined which one was best and at what voltages.

My role in the lab was to determine all these ideal operating parameters. I did so by editing and running the Perl and Matlab scripts, switching chips, setting and resetting power supplies, and a lot of guesswork. It was determined that the chip operated best with a 0.7 volt supply at a 400-500 MHz frequency, with various other more complicated parameters (too complicated to explain here) also determined.

Source Counting and Signal Separation

Elisheva Muskat
Advised under Prof. Sharon Gannot and Mr. Pini Tandeitnik

Blind signal separation (BSS) is separating signals by their sources from a mix of signals without information about the source signals or the mixing process. This can be helpful for analysis of different types of signal related data such as data processing, audio processing, digital communication and image processing.

The focus of the research taking place in Professor Sharon Gannot's lab is on blind source separation of multichannel audio mixtures or BASS. It can be difficult when given a recording of many people speaking over each other such as in a cocktail party or a conference room scenario to single out the speech of a single person. Understanding how to separate these kind of signals can be helpful both for analyzing audio and can have implications for more general BSS.

The lab's proposed method of BASS led by Bracha Laufer consists of a novel approach to diarization which is the process of identifying speakers in a mixed audio signal and then using the results of the diarization to find time time frames in the audio dominated by single speakers and unmix the source signals. While diarization has a clear relation to BASS the lab's approach of BASS is one of the few to address diarization at all.

The novel approach to diarization relies on a probabilistic model which relates the probabilities of the speakers in the audio across time to the column space of the correlation matrix which is a matrix representation of the the ratio between the measurements of the second microphone and the measurements of the first microphone. Therefore the approach is to take the correlation matrix explained above and to find the spectral decomposition which is the correlation matrix represented in terms of its eigenvalues and eigenvectors. The number of speakers corresponds to the number of significant eigenvalues found. The eigenvalues are associated with eigenvectors which make up the simplex of the speaker's activity probabilities by mapping the eigenvectors on to a scatter plot. The number of vertices corresponds to the number of speakers and the points lying near each vertex are associated with frames of the speech dominated by a single speaker.

Based on the diarization outcomes, frames highly dominated by single speakers are found and acoustic channels for individual speakers are estimated. Finally an unmixing scheme is constructed where the individual speakers are

extracted using the pseudo-inverse of the acoustic mixing system.

Another important aspect to testing this algorithm is taking into account reverberation levels. Reverberation level is a measurement of how fast the sound in the room will die which is dependent on how reflectant or absorbent the room. Because acoustics change drastically depending on the reverberation level of the room it's important to have a data set of speakers in rooms of different reverberation levels. Specifically the threshold in determining the amount of speakers may vary depending on whether the reverberation was high or low. If the reverberation is low meaning that sound is mostly absorbed, a lower threshold may be more accurate in evaluating the number of speakers as opposed to higher reverberation where the acoustics are reflected around the room a higher threshold in estimating the number of people in the audio may more be more accurate.

To test this method of BSS the lab has been collecting acoustics of a variety of speakers both male and female in a room of a high reverberation level and a low reverberation level. The lab will then mix the sounds and use the algorithm to separate the source signals with various thresholds to test the accuracy of the algorithm in contrast to other methods of BASS.

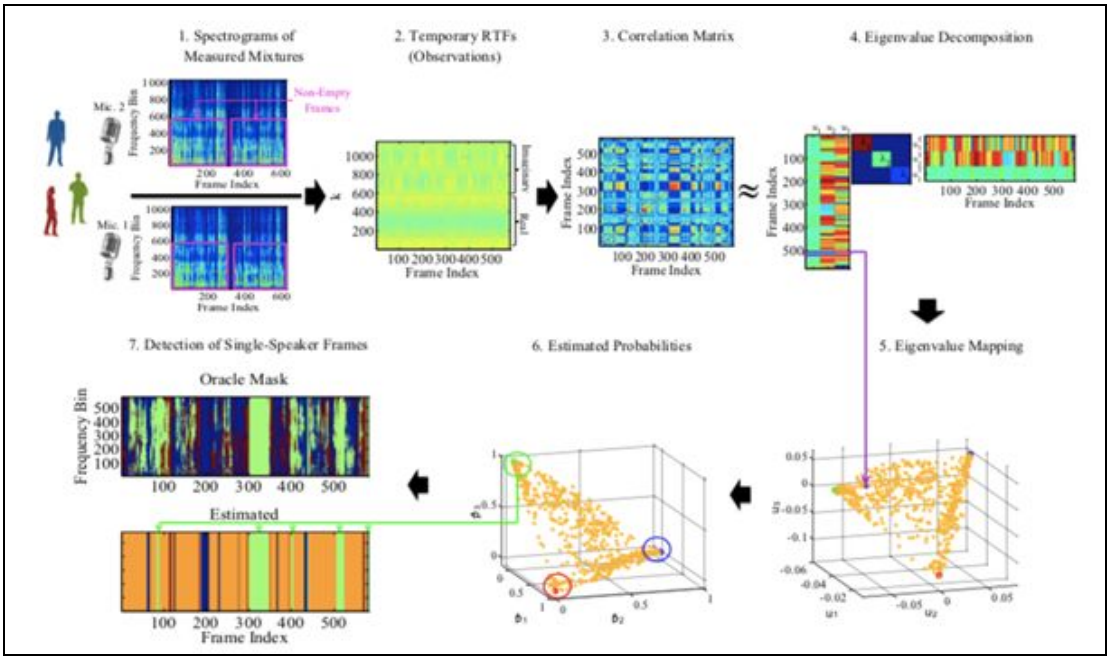

Figure 1: A flow diagram of the proposed diarization method. 1-4 shows the computation of the correlation matrix and the Eigenvalue decomposition. 4-5 shows the Eigenvalue mapping. 5-7 shows the method of estimating the probability of activity of different speakers and the results of the estimation in comparison with the true mask.

Chemistry

(L-R) David Benaroch, Phillip Nagler, Tzivia Linfield, Lauren (Liat) Gorelick, Devorah Saffern

Chemical Vapor Deposition of Nickel Sulfide

Phillip Nagler
Advised under Dr. Daniel Nessim

Chemical vapor deposition (CVD) is a method of reacting substrates at a high temperature in a vacuum of controlled gas flow. Metals are commonly used in CVD and are reacted with gaseous or powdered chemicals. Inert gases are usually flown into the reaction chamber to prevent the oxidation of the metal during the reaction. In Dr. Nessim's lab, I studied the reaction between nickel and sulfur powder in an inert gas environment. The main applications of nickel sulfides are in batteries and fuel cells.

There was a 3-step procedure for the synthesis of nickel sulfide using CVD. Firstly, the reaction chamber was purged with an inert gas for roughly 10 minutes. At this point, the nickel sample and the sulfur powder would not enter the furnace. After the purging is finished, the annealing process was started. The nickel sample is placed into the reaction chamber and hydrogen gas was passed through the chamber to reduce the metal. The time for annealing varied for our different experiments. After the flow of hydrogen gas is complete, the chamber is purged again with a

noble gas before the sulfur powder is placed into the reaction chamber (hydrogen gas reacts with sulfur to create a noxious gas). After the second purge, the third step is placing the sulfur powder into the reaction chamber with the nickel substrate. The amount of time that the sulfur and the metal stayed inside the reaction chamber varied in each experiment.

Very little is known about the reaction mechanism of the nickel sulfide synthesis. Therefore, the reaction conditions are changed from experiment to experiment in order to learn more about the reaction. Many trials were done at different temperatures and different increments of time for the annealing step and reaction step. It was observed that the reaction shows more of a yield when the sulfur is left in the chamber with the nickel sample for longer periods of time. Additionally, when the metal is slowly cooled in the chamber, the morphologies of the products tend to be more uniform.

Once the nickel sulfides are formed, their structures were analyzed using a series of machines. Some of these machines include: E-SEM, AFM, and XRD. The main goal of the lab is to find unique structures and morphologies at the nanoscale. These structures can reveal information about the mechanism of the reactions and can have unique applications for batteries or fuel cells. Once a unique structure is found in a sample, it is sent out to other labs to test its potential applications.

Nanoparticle Polymer Theory for Anti-cancer and Anti-bacterial Treatment

David Benaroch

Advised under Prof. Aharon Gedanken

Intro: With the emerging field of nanotechnology showing great promise in biological faculties, many oncology and infectious disease researchers hope to be able to develop anti-cancer and anti-bacterial compounds with new nanoparticle strategies. With regards to nanotechnology's role in antibacterial research, new techniques of inhibiting opportunistic infections have been discovered and appear to be quite useful. Traditional research with antibacterial compounds strategically target defense mechanisms of infectious organisms by way of chemical inhibition or efflux. This extremely specific therapy is often met with resistance and is ineffective due to the bacteria's ability to either reject the compound's entry into its selectively permeable membrane or to pump it out of the cell before the drug can take effect.

With nanoparticles, scientists can now approach membrane integration much more easily as many recently developed polymers of inorganic compounds have been shown to be effective in serving as an entry way for other drugs into a bacterial cell. This is a method referred to as nanoparticle bridging. Secondly, other nanoparticles are successful in entering the cell and can therefore take immediate action at the cell nucleus, thus affecting cell activities. Both methods are extremely promising and require subsequent investigation.

Summer 2018 Project: After synthesizing various silicon and carbon skeleton polymers, susceptibility testing for compound efficacy against common E. coli and S. aureus strains were conducted. These

are typical organisms used for basic efficacy explorations.

Methods: Agar disc diffusion and mictrotiter broth dilutions were conducted to determine polymer efficacy. Polymers were tested at concentrations ranging from 180 μg- 640 μg for each of 6 polymers and 1 monomer. All compounds were dissolved in PEG which has no antibacterial effect. Additionally, hourly interval checks were made on the broth dilution to test temporal efficacy of the polymers.

Results: After testing efficacy for just the polymer itself, no antibacterial effect was shown. Adding metal oxide compounds to the nanoparticle structure of the polymer did however show efficacy after subsequent testing. Electron Paramagnetic Resonance images of the polymers, metal oxide compounds, and the two combined demonstrated a synergistic effect meaning there was an increased antibacterial effect. Specifically, polyaniline in combination with zinc copper oxide showed efficacy.

Conclusion: Based on this summer's results, the Gedanken lab of Bar-Ilan University sees great promise in using nanoparticle compounds as potential antibacterial therapies. Subsequent modifications and testing will ensue and correspondence between my lab in the Veteran Affairs Hospital of Syracuse, New York and the Gedanken lab will surely occur in the near future.

Immunoglobulin Variable Light Chain Causes Amyloid Fibril Formation in SMA Protein

Tzivia Linfield
Advised under Prof. Jordan Chill and Dr. Hadassa Shaked

Systemic light chain amyloidosis (AL) is the most common form of amyloidosis. It occurs when immunoglobulin light chains (V_L), produced in the bone marrow, and released to the plasma, misfold and aggregate throughout the body, negatively affecting many internal organs. When misfolded, V_L chains form oligomers and fibrils; this aggregated form interacts with a variety of membranes, generating channels and pores that lead to cell toxicity.

SMA and LEN are homologous V_L chain proteins. SMA forms cytotoxic fibrils, while LEN does not. These proteins will serve as an experimental system to develop inhibitors for V_L chain aggregation, in order to reduce their concentration and toxicity. Our project focuses on cloning, expression, and purification of SMA and LEN.

The genes for LEN and SMA immunoglobulin V_L chains were inserted using G-block technology into a pET28 plasmid. They were then used to transform competent Escherichia Coli cells (BL21 strain). Cells were lysed using sonication and screened on SDS-PAGE for protein expression. Both LEN and SMA showed high expression as insoluble inclusion bodies. In order to transform this non-native form of the proteins to usable soluble V_L domains, the insoluble proteins were denatured using 8 M urea and purified on a nickel affinity column. The eluted protein was then dialyzed against buffers containing decreasing concentrations of urea, gradually removing all urea and DTT. SDS-PAGE analysis confirmed about 10% of properly refolded protein. Size exclusion chromatography further confirmed the presence of properly folded monomers.

In order to encourage the protein to refold properly as soluble protein in cytoplasm of the bacterial cells, conditions for overnight induction were altered. Results showed minimal expression in the supernatant of the cells which were grown in Luria-Bertani Broth (LB) overnight at 16 °C with 0.05mM IPTG. The supernatant was then purified on nickel beads. SDS-PAGE of the purified protein showed very low expression. More conditions will be tested to encourage the protein to solubilize and

express in the cytoplasm. Additional option is to express the folded protein in the periplasm of the cell by introducing a new vector with a signal peptide that encourages the protein to enter the periplasm, where it can easily be folded.

Once the protein is purified in higher amounts in its native fold, NMR spectroscopy will be used to better understand the structure of the V_L. Various compounds will then be tested to determine the most effective way to develop a therapeutic treatment of systemic light chain amyloidosis.

References:

Brumshtein, B.; Esswein, S. R.; Landau, M.; Ryan, C. M.; Whitelegge, J. P.; Phillips, M. L.; Cascio, D.; Sawaya, M. R.; Eisenberg, D. S. Formation of amyloid fibers by monomeric light chain variable domains. *J. Biol. Chem.* 2014, 289, 27513-25.

Bucciantini, M.; Giannoni, E.; Chiti, F.; Baroni, F.; Formigli, L.; Zurdo, J.; Taddei, N.; Ramponi, G.; Dobson, C. M.; Stefani, M. Inherent toxicity of aggregates implies a common mechanism for protein misfolding diseases. *Nature* 2002, 416, 507-11.

Clos, A. L.; Lasagna-Reeves, C. A.; Castillo-Carranza, D. L.; Sengupta, U.; Jackson, G. R.; Kelly, B.; Beachkofsky, T. M.; Kayed, R. Formation of immunoglobulin light chain amyloid oligomers in primary cutaneous nodular amyloidosis. *Br. J. Dermatol.* 2011, 165, 1349-54.

Ionescu-Zanetti, C.; Khurana, R.; Gillespie, J. R.; Petrick, J. S.; Trabachino, L. C.; Minert, L. J.; Carter, S. A.; Fink, A. L. Monitoring the assembly of Ig light-chain amyloid fibrils by atomic force microscopy. *Proc. Natl. Acad. Sci. U. S. A.* 1999, 96, 13175-9.

Laganowsky, A.; Liu, C.; Sawaya, M. R.; Whitelegge, J. P.; Park, J.; Zhao, M.; Pensalfini, A.; Soriaga, A. B.; Landau, M.; Teng, P. K.; Cascio, D.; Glabe, C.; Eisenberg, D. Atomic view of a toxic amyloid small oligomer. *Science* 2012, 335, 1228-31.

Schmidt, A.; Annamalai, K.; Schmidt, M.; Grigorieff, N.; Fandrich, M. Cryo-EM reveals the steric zipper structure of a light chain-derived amyloid fibril. *Proc. Natl. Acad. Sci. U. S. A.* 2016, 113, 6200-5.

Developing an Accelerated Pathway for Synthetic Retinal A

Lauren (Liat) Gorelick
Advised under Prof. Arie-Lev Gruzman
PhD student Lena Trifonov

Retinitis Pigmentosa (RP) is a retinal degenerative disease in which human eye's rod photoreceptors are broken down and lost. This can have a dramatic effect both on a person's peripheral vision and low light vision. A variety of retinal molecular pathway defects have been matched to multiple known RP gene mutations. Professor Gruzman's lab is looking to develop a shortened (7-8 steps) synthetic route to cis-C(11)-locked retinals A to be used for treatment of this disease. Although any of the desirable compounds, i.e. retinal A and retinal B, could be prepared through the very long and laborious published procedures, the abridging of the overall synthetic routes would be favorable for the reasonable access to retinoids A and B. The curtailing of the synthesis of cis-C(11)-locked retinals A by means of minimization functional group (FG) interconversions (FGI) is presented in Figure 1 below.

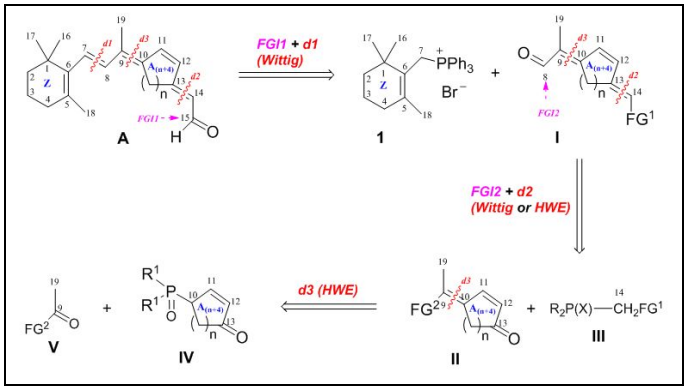

Figure 1: A minimizing functional group (FG) interconversions (FGI) general retrosynthetic approach to the target cis-C(11)-locked retinals A. Additional abbreviations: d – disconnection (dislocation); HWE - Horner–Wadsworth–Emmons olefination.

According to this retrosynthetic analysis, all the target cis-C(11)-locked retinals A could be derived through 3 common sequential

disconnection (d) of the C(7)=C(8), C(13)=C(14) and C(9)=C(10) double bonds accompanied with 2 (or 3) requisite FGI from the corresponding alicyclic unsaturated δ-ketophosphonates (if R1= AlkO) or –phosphinoxides (R1= Ph) IV and pyruvic acid derivatives V (Scheme 1). As in all but one reported so far syntheses of cis-locked retinals A the assemblings of the listed above C=C bonds is planned to accomplish using phosphorus chemistry, namely Wittig and/or Horner–Wadsworth–Emmons (HWE) olefination. A supplementary Peterson olefination with silylated acetaldehyde tert-butylimine anion was fruitful for the final construction of C(13)=C(14) bond in the early syntheses of cyclopenteno-retinals A5. However, in the syntheses of 8- and 9-membered retinals A8,9 similar Peterson olefinations were reported to be infertile. Probably, this silicon alternative should not be considered as a method of choice in the further optimization design.

In contrast to all the reported before syntheses of the cis-C(11)-locked retinals A our synthetic plan supposes the last assembling of the C(7)=C(8) bonds rather than final formation of the C(13)=C(14) bonds. Upon appropriate choice of the convertible to carbonyls FGs, such a selection provides with the possibility of shortening overall synthetic route through the less extensive FGIs in the containing A(n+4)-ring early stage precursors such as IV, etc. We hope this route allows less time- and labor-consuming production of the target retinals A as we hope to achieve a more efficient treatment of Retinitis Pigmentosa.

Synthesis and Characterization of Hierarchical Structures Formed from Amino Acid Blends

Devorah Saffern
Advised under Prof. Yitzhak Mastai and Dr. Michal Ejgenberg

Previous research has shown that certain amino acids form hierarchical structures in spherical shapes when crystallized. These organic crystals, which are made of smaller repeating crystals arranged in a periodic way, are among the work being studied in Professor Mastai's lab. Other past published literature described a single amino acid mixed with a polymer, while Professor Mastai's lab began testing blends of two amino acids. Those tests showed that spherical structures can form from mixtures of L-Glutamic Acid and L-Arginine dissolved in miscible ethanol-water solvents.[2] The proposed mechanism of sphere formation involved electrostatic interactions between the charged carboxyl group of glutamic acid and arginine's positive charge.

The goal of this experiment was to find more structures possessing this spherical morphology and to try to understand the mechanism by which they form. Various combinations of amino acids were analyzed to determine the effects of electrostatic attraction and repulsion on structure formation. The amino acids were dissolved in water and combined with ethanol, an anti-solvent that led to formation of a quasi-emulsion of water droplets highly saturated with the amino acid, suspended in the ethanol. Phenylalanine was tested with both tryptophan and tyrosine to detect whether π stacking due to their aromatic rings could lead to a unique formation, but no spheres formed. The combinations found that contained spheres under

[2] Nemstov, Irena, Mastai, Yitzhak, & Ejgenberg, Michal. (2018). Formation of Hierarchical Structures of L-Glutamic Acid with an L-Arginine Additive. Crystal Growth and Design, 18 (7), 4054-4059.

our experimental conditions were crystals made from solutions of glutamine with low concentrations of arginine, as well as asparagine with arginine. The samples were analyzed using Environmental Scanning Electron Microscopy (E-SEM) to detect the spheres.

Certain experimental conditions were changed to optimize sphere formation. After testing varying ratios of ethanol and water solvents, we determined that increasing the amount of ethanol yielded more perfectly shaped, smaller spheres of the glutamine-arginine blend (10 mL ethanol: 1 mL water, 20:1, and 30:1 were tested), based on optical images and E-SEM. Asparagine-arginine blends produced best results when dissolved in a 50:1 ethanol to water ratio. Further directions include testing more combinations of amino acids that form spheres, in order to better understand the mechanism. In addition, perhaps other solvents can be tested – we analyzed acetone, which had little to no spherical structure, but perhaps other solvents would work. We found under the pH conditions in our experiment that the acids are not charged while the amine groups are, so there are no oppositely charged pairs to create electrostatic interactions; attractive or repulsive electrostatic forces are therefore likely not the cause of spherical formation in the samples we prepared. The mechanism of spherical formation is then unknown, and further work would involve better understanding this process by continuing to vary experimental parameters and note structural changes.

This work has potential applications in the pharmaceutical industry, since spherical crystals can be used in the production of tablets, as shown in previous research. Spherical crystallization is a technique that involves crystallization and agglomeration, to yield better flow behaviors, solubility, size, etc. of components of a drug.[3,4] Understanding the mechanism of sphere formation could enable further use of spherical crystallization and improve pharmaceutical production techniques.

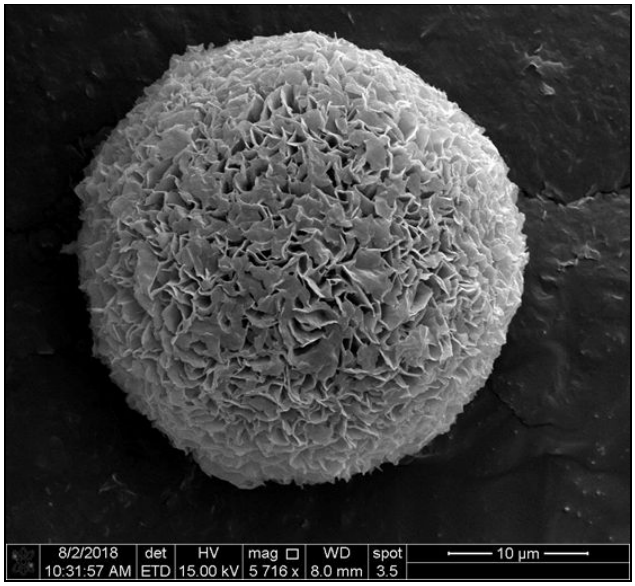

Figure 1: Electron Microscopy image of Glutamine-Arginine blend crystal dissolved in 30:1 ethanol-water solution

[3] Chatterjee, A., Gupta, M. M., & Srivastava, B. (2017). Spherical crystallization: A technique use to reform solubility and flow property of active pharmaceutical ingredients. *International Journal of Pharmaceutical Investigation*, 7(1), 4–9. http://doi.org/10.4103/jphi.JPHI_36_16

[4] Saini, Sumant. (2014). Spherical Crystallization: An Overview. *International Journal of Drug Delivery Technology* 4(4), 72-80.

Life Sciences

(L-R) Ariel Kohenbash, Devorah Lamm, Ariella Gordon, Allison Schachter, Ester Shavalian

The effects of T294 phosphorylation in SIRT6

Devorah Lamm
Advised under Prof. Haim Cohen and PhD student Matan Avivi

As the scientific community continues to create innovative ways to combat disease, the average human lifespan has increased. With longevity, however, comes a litany of age related disorders including diabetes, obesity, generalized inflammation, and cancer. The question is, then, how to promote longevity while avoiding its natural consequences. The answer, it seems, may reside with the protein, SIRT6.

Prof. Haim Cohen's lab studies the mammalian sirtuins, homologs of the age regulating Sir2 protein found in yeasts. The lab has specifically looked at SIRT6, a NAD+ dependent, chromatin-associated deacylase, which affects the expression of multiple genes. SIRT6 has been implicated in the regulation of aging-related pathways, including inflammation, glucose metabolism, and genome stability. In previous studies, Prof. Cohen's lab has demonstrated that male mice genetically modified to overexpress SIRT6 have increased health and an increased lifespan. Conversely, SIRT6 KO mice develop a series of aging related diseases and have shortened lifespans.

Post-translational modifications are very important for protein regulation. SIRT6 T294 undergoes phosphorylation on humans and primates, however, the function of this phosphorylation has yet to be elucidated.

In my research, I was a part of a team that studies the function of the phosphorylated T294 as it relates to its activity, interactions, and localization pattern. In order to reveal if this phosphorylation is related to SIRT6 activity, our team created a recombinant protein containing an aspartic acid on T294 which mimics phosphorylation. Our objective is to check its activity in purified chromatin histones. My goal

was to extract chromatin histones from HEK293T WT and SIRT6 KO cells, validate them and determine the samples' purification.

After extracting the chromatin histones, I determined via Coomassie staining that there were impurities in the samples. Using a Western Blot, I tried to determine which proteins were in my sample other than H3, as these proteins may affect a future activity assay with SIRT6. Likely candidates included proteins other than H3, such as, SIRT6 itself, SIRT1, LAMINA, and PARP1/2. After analyzing several Western Blots, I determined that LAMINA and PARP1/2 were present in the chromatin histone samples. Both of these proteins are known to interact with SIRT6, thus, it is imperative that their effect be taken into account during a future activity assay.

Genome Editing to Reverse the "Bubble Boy" disease

Ariel Kohenbash
Advised under Dr. Ayal Hendel and Dr. Adi Tovin

Background: Severe combined immunodeficiency (SCID, also known as "Bubble Boy" disease), is a recessive genetic disorder characterized by the disturbed development of functional T and B cells caused by genetic mutations of several different genes, of which include the RAG1 and IL7RA genes. While allogeneic bone marrow transplantation can be curative for these disorders, there remain significant limitations to this approach. A potential cure for such monogenic disorders can be the transplantation of autologous gene-corrected hematopoietic stem cells (HSCs). Dr. Hendel's lab focuses on developing CRISPR (Clustered Regularly Interspaced Short Palindromic Repeats) genome editing as a platform for innovative curative gene correction therapies for SCID disorders.

CRISPR has revolutionized the realm of genome editing which has led to new approaches to curing monogenic diseases. The CRISPR complex consists of two parts, the guide RNA (gRNA), and the Cas9 nuclease protein. The gRNA allows the DNA endonuclease, the Cas9, to target specific nucleotide sequences in a genome. The DNA target is recognized by the Cas9-gRNA complex through Watson-Crick base pairing interactions. Once the gRNA successfully attaches to the targeted nucleotide sequence, the Cas9 protein creates a double-stranded break (DSB). Once the cut has been made, the cell can repair the break in one of two basic mechanisms. The first, nonhomologous end-joining (NHEJ), usually leads to repairs that can create insertions or deletions (indels) at the site of the break. The second, homologous recombination (HR), can be exploited to incorporate a desired genomic alternation in the presence of a suitable DNA donor. SCIDs can potentially be cured via HR in the presence of a donor DNA sequence bearing the corrected cDNA sequence of the disease-causing gene.

Aim: The goal of this project was to design and construct donor DNA plasmids that will serve as a template to model and correct mutations of the RAG1 and IL7RA genes in HSCs. The first group of these plasmids is termed "disruption plasmids". These plasmids contain fluorescent markers (GFP or tdTomato) in between the left and right homology arms sequences of each gene. These markers will be knocked into the genome to disrupt the endogenous gene sequence. This will allow us to model the SCID disease. The second group of plasmids contains the correct sequence of each gene cDNA. These plasmids will serve as the template for the HR machinery to knock-in the RAG1 and IL7RA WT cDNA and correct the patient's mutations. Our hypothesis is that the cells that were disrupted by the two fluorescent markers will not become functional T or B cells.

The plasmids containing the WT cDNA will be used to determine if the corrected sequence can effectively reverse the disease and lead to normal development of functional T and B cells.

Method and Results: Primers were designed to amplify the left and right homology arms along

with the fluorescent markers for each of the donor DNA plasmids. Using PCR, the homology region of IL7RA and RAG1 were amplified along with the fluorescent markers (GFP and tdTomato) used for disruption. PCR products were run on 1% agarose gel. The correct PCR product was extracted from the gel and was then purified. The clean PCR products were inserted into a plasmid vector using the NEBuilder HiFi DNA Assembly Cloning Kit (New England Biolabs, MA, USA). The plasmids were then transformed into competent E. Coli bacteria and spread onto plates containing agar and ampicillin. These plates were left at 37°C overnight. For each construct, eight bacterial colonies were grown in liquid LB and the plasmids were extracted by GeneJET Plasmid Miniprep Kit (Thermo Fisher Scientific, MA, USA). The cloned plasmids were then screened by restriction enzyme digestion to test if the correct plasmids were constructed. The positive clones were then sequenced by Sanger sequencing for final verification. The plasmids that were designed to disrupt the RAG1 and IL7RA gene using GFP and tdTomato yielded successful plasmid product. These described plasmids will be used in the future by Dr. Hendel's lab to model and reverse the SCID disease.

Summary: Genome editing was suggested as a therapeutic method for diseases such as SCID more than a decade ago. With the CRISPR revolution, this dream is getting closer and closer. To date, there is still limited data on the utility of CRISPR systems in human therapeutics, but studies are on their way including proof of concept studies in animal models and human cells in many labs, including Hendel's lab. Further experience is still required to evaluate the outcomes and long-term effects of CRISPR genome editing for human therapeutics but based on the vast amounts of effort being invested by the scientific biomedical community, the future of therapeutic genome editing looks promising.

The Influence of Intrauterine Position and Paternity on Fetal Testosterone and Cortisol Levels in Nutria.

Ester Shavalian
Advised under Dr. Lee Koren and PhD student Ruth Fishman

In over 130 species, including insects and mammals, mating with multiple partners is not uncommon and might even strengthen male reproductive success, while female reproductive success is determined by the number of ova produced and offspring raised. There are many drawbacks of multiple paternity for females including increased exposure to sexually transmitted diseases and vulnerability to predation and injuries from potential mating partners. Genetic benefits from multiple mating is very varied including benefitting good genes from extra pair males and genetic compatibility. Another direct benefit of multiple mating is in the form of fertility insurance, like an influx of male resources and and a decrease in male aggressiveness.

The research I was involved in used a very large sample, containing hundreds of pregnant nutria cadavers that were attained through culling. Our research was used to investigate whether there was an association between multiple paternity and litter size- do litters with higher frequency of multiple paternity differ in their size from single paternity litters? We also wanted to see if there was an association between multiple paternity and sex ratio- do the litters with more fathers different in their sex ratios from single-father litters? Lastly, we wanted to see if there was an association between multiple paternity and fetal morphology.-would fetuses from different fathers differ in their morphological characteristics?

We first took morphological measurements from the pregnant mothers. Then we exposed the uterus and recorded the IUP of the uterus, took

measurements and shaved the hair for T and cortisol quantification. Tail clippings were excised from the fetus for DNA extraction and were preserved in 70% ethanol and kept in -80 degrees Celsius until processing. We isolated total DNA from 20 mg of tail tissue. We then used a 800µL lysis buffer to do cell cell lysis and then added 8µL Proteinase K, and put in water bath at 55 degrees Celcius for two hours. After 10 minutes of centrifugation at -4°C, the supernatant was collected and 400µL of isopropanol was added to the tubes, vortexed, the supernatant was removed and the tubes were left at room temperature to evaporate the isopropanol leftovers. The DNA was then suspended in 100µL ddH2O. DNA concentration and cleanness were checked by NanoDrop and diluted as necessary. All PCR reactions were performed in the following program: initial denaturation at 94 °C for 2 min; 35 cycles of 94 °C for 30 s, 56 °C for 30 s, 72 °C for 1 min; and a final extension at 72 °C. Initial microsatellite analysis was performed on 297 fetuses, from 55 litters.This allowed a preliminary siblicity analysis that has revealed that out of 21 mothers examined at least in 9 liters there was multiple paternity (more than 1 genetic father). This result demonstrates our ability to exclude full siblicity and that nutria is an adequate model to examine the forces related multiple paternity.

The Effects of SNF5 on Pluripotent Stem Cells

Ariella Gordon
Advised under Dr. Achia Urbach
and PhD student Ilana Gross Carmel

Pluripotent stem cells (PSCs), both embryonic and induced stem cells, are unique in their capacity of self-renewal and their ability to differentiate into all cells that form an organism. The smallest changes in external and internal signals can start signal transduction in these cells, which eventually will lead to changes in transcription and epigenetic factors that control the balance between self-renewal and differentiation of PSCs.

One of the epigenetic factors in cells is the SWI/SNF complex. SWI/SNF complex is an ATP dependent chromatin remodeler that consists of ten to twelve subunits. Although different cell types have different compositions of these subunits, there are core subunits that are found in every cell type, such as the catalytic ATPase subunit BRG1 or BRM, BAF155, BAF170 and SNF5. DNA remodeling plays a key role in tumor suppression, as loss of function mutations in at least one subunit of the SWI/SNF complex were reported in various cancers. In 98% of Rhabdoid tumors, an aggressive pediatric tumor of the kidney or the brain, SNF5 depletion is the sole genetic aberration.

By using embryonic stem cells with conditional SNF5 knock-out, the cells' morphological changes and gene expression were observed. Additionally, doxycycline was removed from knock-in knock-out cells (KIKO). Doxycycline is an antibiotic which sits on a transcription factor and inhibits SNF expression.

SNF5 expression is depleted when doxycycline is removed from KIKO cells. These cells also curiously detached from the plate. It is imperative to study the effects of the SNF5 gene in order to comprehend the differentiation pathway all the way to the tumor. Numerous experiments are being performed, with the aid of real time PCR, in order to analyze various genes involved and affected by SNF5.

PCR, or polymerase chain reaction, amplifies cDNA which is complementary to mRNA. A large number of differentiation genes from all three germ layers were analyzed, and the results confirmed there is indeed differentiation. A question to be addressed was whether the detachment was a result of differentiation or the cause of it?

The cells that were without doxycycline for 72 hours did not show SNF5 expression yet were

still attached to the plate. Considering there may be an aberration with cellular adhesion, adhesion markers were analyzed. The PCR analysis did not show sufficient enough differences between differentiation and adhesion markers. In order to continue the research, cells with new time frames were used.

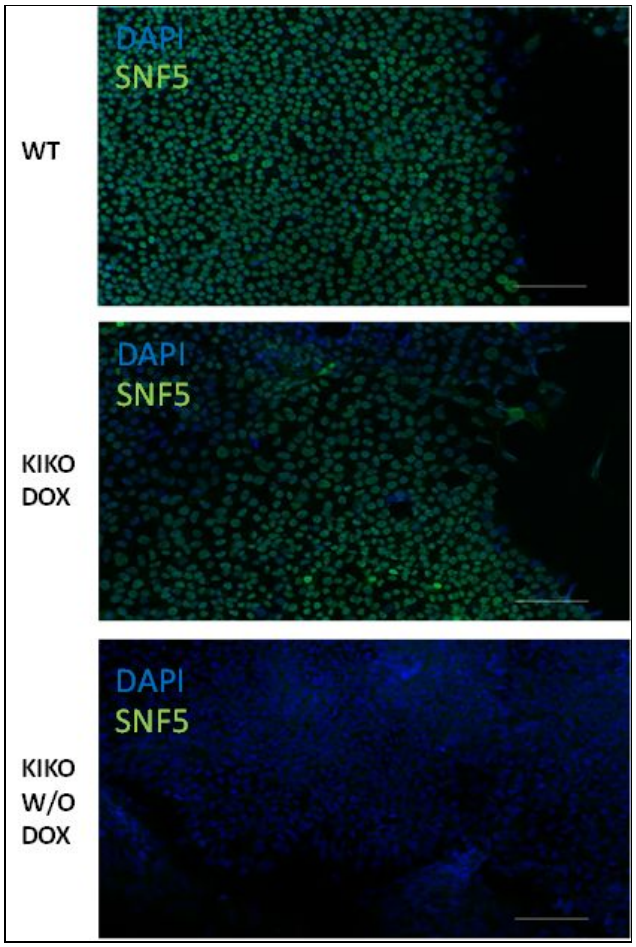

A specific gene being analyzed, LOXL1 shows a slight decrease in the KIKO cells without doxycycline. This decrease suggests there is first detachment, which then allows for signal transduction, causing differentiation. Continuing in this direction, new cells are being used with a longer time frame in order to confirm the hypothesis.

Chemotherapy Induced Stress Granules and the Effects of their Inhibition

Allison Schachter
Advised under Prof. Yaron Shav-Tal and PhD student Avital Gross-Schwed

Several disruptive conditions, such as heat, nutrient deprivation, UV radiation, and oxidative stress can disturb cell homeostasis and cause cellular damage. One way in which cells cope with these stressful environments is through the production of cytoplasmic stress granules, which form as a result of cellular inhibition of translation initiation in order to conserve energy. Stress granules also serve as signaling centers for the cell, and can up or downregulate factors essential for survival, depending on the composition.

In the treatment of tumor cells, chemotherapy can induce stress granule formation, the presence of which has been shown to promote tumor metastasis and survival. This can interfere with the treatment potential, and result in cells resistant to that particular chemotherapy continuing to thrive. Interfering with the production of stress granules, therefore, could potentially increase the potency of the chemotherapy and prevent continuing growth. Not all stress granules have this capability, as those that are pro-apoptotic would have the opposite effect to those that were pro-survival, necessitating characterization of the stress granules induced by differing chemotherapies. Our lab studied the effects of three different chemotherapies on U2OS cells, and found that the stress granules induced by selenite differ from those from tubercidin and vinorelbine in that they lack eIF3, the downregulation of which results in an increase of pro-apoptotic factors. Those induced by tubercidin and vinorelbine, on the other hand, contain eIF3, and therefore result in increased cell survival.

In order to block the formation of stress granules, our lab studied the effects of two different compounds, factor C and glycogen synthesis kinase, also known as Gsk. Using immunofluorescence, we observed that cytoplasmic stress granules were present in cells treated with all three types of chemotherapy. When factor C and Gsk were added in combination with tubercidin, we observed complete stress granule inhibition. In selenite, however, factor C and Gsk reduced stress granule formation only slightly, and vinorelbine treated cells responded differently to the two compounds— Gsk reduced the number of stressed granules, but factor C caused an increase. These varying responses to stress granule inhibition factors indicate a differing mechanism of the chemotherapeutic compounds, requiring further study. We are additionally studying the effects of factor C and Gsk on cells treated with sorfanib, another chemotherapy shown to induce pro-survival stress granules.

To test the impact of stress granule inhibition on cell survival, XTT assays were performed on cells treated with tubercidin and vinorelbine in conjunction with factor C and GSK. All cells treated with the chemotherapy, whether alone or in combination, had an almost complete decrease in cell viability. The addition of stress granule inhibition compounds produced a slight increase in cell viability, especially in tubercidin and factor C, but these effects became less pronounced over the course of 72 hours, and in all other combinations the differences were too small to indicate significant results.

In the future, our lab aims to produce chemo resistant cells through repeatedly treating cells with the chemotherapy and allowing those that survive to grow, in order to observe the effect of factor C and Gsk on resistant cell viability. We also aim to test the effects of these compounds on cells treated with sorfanib. Additionally, we aim to further understand the mechanism of factor C in relation to stress granules, and how it interacts with the differing chemotherapies, furthering our understanding of stress granule effects within tumor cells.

Mathematics, Computer Science and Physics

Back (L-R): Joseph Rubin, Mark Kaplan, Jacob Stern.
Front (L-R): Chana Tropp, Avital (Tali) Greenberg

Analyzing the Twitter Follow Graph to Determine if it is a Social Network or Information Network

Avital (Tali) Greenberg
Advised under the lab of Prof. Liam Roditty

Twitter as a media platform continuously begs the question: is it a social network or an informational network? The standard Twitter follow relationship is primarily about consuming information, but still many follows are built on social ties. By characterizing the topological features of the Twitter follow graph and comparing them to available data from other social networks, we can argue that it is indeed a hybrid network.

Social networks and informational networks have different trends in specific properties of their follow graphs that allows for proper characterization. My research included analyzing properties of the Twitter graph such as degree distributions, connected components, shortest path lengths, clustering coefficients, two-hop neighborhoods, and degree assortativity using a Python module called Networkx. A social

network's goal is towards sharing personal and professional experiences with a user's friends. Therefore, a social network's follow graph tends to exhibit properties such as high degree assortativity, small shortest path lengths, large connected components, high clustering coefficients, and a high degree of reciprocity. An informational network's goal is towards the dissemination of information and the dominant interaction is following those who provide information users want. Its follow graph tends to exhibit properties such as large vertex degrees, lack of reciprocity, and large two-hop neighborhoods.

My analysis found that the Twitter follow graph has some attributes consistent with social networks and other characteristics consistent with information networks. The average discrepancy between in degree and out degree of each vertex, representing the number of followers and friends a user has, respectively, implies that Twitter is not a social network since it is highly unlikely that users can maintain the amount of social relationships as the number of outbound edges suggest. Additionally, the largest strongly connected component of the graph only contains 84% of all vertices in the graph. This is less than a standard social network; it implies that many edges in the graph are not reciprocated, meaning that users only follow other users for information dissemination or consumption and not to maintain social relationships. On the other hand, the average shortest path length of the graph is shorter than that of Facebook and tends to decrease with size, suggesting that Twitter does behave like a social network. Similarly, I have found that the average clustering coefficient amongst vertices with different degrees is consistent with expectations of a social network.

The results of analyzing these topological characteristics of the Twitter follow graph present that Twitter behaves like a social network in some ways and an informational network in other ways. This hybrid network characterization implies that Twitter users have different motivations for using the platform. Twitter users can utilize Twitter to absorb and circulate information and ideas, as well as connect with friends and establish communities.

The results from my research were based off a Twitter dataset from the Stanford Network Analysis Project that contained a portion of the Twitter graph using data crawled from public sources. The next step in my project was to run this analysis on a more recent model of the Twitter follow graph. I connected to the Twitter API and used a Python module called Tweepy to harvest real Twitter users and wrote custom code to create a small sample of an updated Twitter graph. The continuation of this project would be to analyze the characteristics of this graph to identify if the structure of the Twitter follow graph has changed over time.

This research was adapted from research done by Myers, Seth A, et al. "Information Network or Social Network?: The Structure of the Twitter Follow Graph." ACM, *Proceedings of the 23rd International Conference on World Wide Web*, 2014, pp. 493–498

In search of Zeta Functions Over Maximal Class Lie Rings Through Canonical Forms of P-adic Matrices

Jacob Stern
Advised under Dr. Michael Schein

It has been known since Euler that $\zeta(s)_{\mathbb{Z}} = \prod_{p \in P} \frac{1}{1-p^{-s}}$, P being the set of all primes. In 1988 this was generalized to all finitely generated torsion-free nilpotent groups. Most notably for this paper the Zeta Function over $\mathbb{Z}^n$, $\zeta_{\mathbb{Z}^n}(s)$ can be broken down into P-adic components. In essence $\zeta(s)_{\mathbb{Z}^n} = \prod_{p \in P} \zeta_{\mathbb{Z}_p{}^n}(s)$. The search among leading mathematicians in the field is to find a general solution to the Zeta function of general nilpotent Lie rings. That is rings of any dimension n and any nilpotency class. As with many fields in mathematics in order to find a general solution, one must start out working on small particular solutions. To be more precise, mathematicians are trying to count ideal submodules of a free module generated by n elements, over the P-Adic integers $\mathbb{Z}_p$ for some fixed p with some bracketing operation that satisfies the standard axioms for a Lie Algebra. In the past the only way of calculating this was through a P-Adic Integral, and the messy analysis that that would entail. In recent years however, Doctor Michael Schein possibly amongst others, have discovered a new way of computing $\zeta_{\mathbb{Z}_p{}^n}(s)$.

Note: Although $\zeta_{\mathbb{Z}_p{}^n}(s)$ traditionally refers to the Zeta Function on an Abelian Lie Ring over $\mathbb{Z}_p$, in this paper it will refer to a Zeta Function on any Lie Ring over $\mathbb{Z}_p$.

This new method starts by taking ring of nxn P-adic matrices in Hermite Normal Form i.e. upper triangular matrices with diagonal elements in the form of p^{a_i} and all non zero elements in the column of p^{a_i} contained in the group of coset representatives of $\frac{\mathbb{Z}_p}{p^{a_i}\mathbb{Z}_p}$. The exponents in the diagonal form a vector A = $(a_0, a_{1\ldots a_{n-1}})$. Next conditions are imposed on those matrices so that the submodule generated by its row vectors is an ideal of the Lie ring generated over $\mathbb{Z}_p{}^n$. Any matrices satisfying all those conditions will "contribute" its determinant to the Zeta Function. So one ends up with the formula $\zeta_{\mathbb{Z}_p{}^n}(s) = \sum_{A \in N} p^{L(A)} \{p^{(a_0+a_{1+\ldots a_{n-1}})}\}^{-s}$ with the condition $A \in N$ becoming stricter if there are restrictions of the diagonal elements. That "strictness" ends up creating a lot of complexity, and is what contributes the most to the difficulty of this method. Utilizing this method allows for a simpler linear algebra based solution to a seemingly much more complicated analysis problem.

My work this summer was to study Lie algebras of n dimensions and nilpotency class $n-1$. Generated by the n elements $x_0, x_1 \ldots x_{n-1}$ defined with the bracketing operation such that $x_i \; i \neq 0, n-1 \quad [x_0, x_i] = x_{i+1}$ with all other brackets commuting i.e. equaling zero. The goal was to hopefully streamline the process, or attack it from a new angle.

For Lie Rings with nilpotency class 1 (Abelian Lie Rings) or Generalized Heisenberg Lie Rings (a subset of the Lie Rings with nilpotency class 2) the solution is almost trivial. For Abelian rings for some fixed p and n $\zeta_{\mathbb{Z}_p{}^n}(s) = \prod_{i=0}^{n-1} \frac{1}{1-p^{i-s}}$. For Generalized Heisenberg Lie Rings $\zeta_{\mathbb{Z}_p{}^n}(s) = \left[\prod_{i=0}^{n-2} \frac{1}{1-p^{i-s}}\right]\left(\frac{1}{1-p^{n-1-3s}}\right)$. However once

we get to nilpotency classes higher than that, things start getting much trickier.

My research this summer was to begin work specifically on the Lie ring M_5. The module is generated by $x_0, x_1, x_2, x_3, x_4, x_5$ such that $x_i\ i\neq 0, 5\ \ [x_0, x_i] = x_{i+1}$ with all other brackets commuting i.e. equaling zero. While the work is not yet completed, so far conditions have been found for all elements other than p^{a_0}.

Power-Law Correlations in Wrist Actigraphy Data of Healthy Subjects and Patients with Traumatic Brain Injury

Mark Kaplan
Chana Tropp
Advised under Dr. Ronny Bartsch

Human motor activity is inherently complex, being affected by numerous factors both extrinsic (normal physical activity, sports, response to random events) and intrinsic (the circadian rhythm, sleep/wake cycles). Traditionally, the output signals of motor activity such as wrist actigraphy data have been considered as random noise and often ignored. However, recent studies have found long-range power-law correlations and nonlinear features in such data, which are consistent among healthy individuals (independent of their activity level) but break down in patients with Alzheimer's disease. These findings indicate that human activity control may be based on a multiple-component nonlinear feedback mechanism encompassing coupled neuronal nodes located in the central and peripheral nervous systems. Moreover, the results also suggest that statistical physics measures that quantify power-law correlations and nonlinear properties could be used as diagnostic markers and to monitor treatment for patients with neurodegenerative diseases or acute injuries of the central/peripheral nervous system.

The overall goal of our project is to investigate statistical physics measures that characterize scaling and correlation properties of actigraphy fluctuations in order to monitor the rehabilitation of patients with Traumatic Brain Injury (TBI). The project also includes the long-term recording of actigraphy data (~7-10 days) from several healthy subjects and patients before and after treatment. This is an interdisciplinary project that combines the application of advanced physics methods for data analysis with long-term recording at the BIU Physics Department and work with medical doctors and clinicians at Sheba Medical Center to record the data.

Since human activity is largely influenced by the central nervous system, we hypothesize that patients suffering from Traumatic Brain Injury (TBI) would show different activity patterns as a result of their injury. To address this hypothesis, we recorded data from healthy subjects (n=2) as well as patient with TBI (n=2). Moreover, we developed computer programs for data analysis to utilize, for example, the detrended fluctuation analysis (DFA). Detrended fluctuation analysis is a method used to determine the self-affinity of a signal. The DFA produces an exponent, α, which indicates the correlation, or conversely the randomness, of a certain signal. Before applying the programs to analyze the physiological data, we performed tests on artificially generated surrogate data using the Fourier-filtering method .

Figure 1a shows an example of wrist actigraphy data of a healthy subject recorded continuously over 7 consecutive days of normal activity. The DFA exponent α for this data is 1.0 (Fig. 1c), a value that corresponds to 1/f behavior, which is characteristic for healthy human motor activity. Shuffling the data and hence destroying any correlations, yields $\alpha = 0.5$ (Fig. 1b and Fig. 1c, green curve). In Fig. 2 we depict the data of one TBI patient. Data was analyzed separately for each

24h period and sorted by the overall level of activity during those days. Note that despite the significant difference in the activity levels for different days, the DFA exponent α is unaffected and shows a almost constant value of $\alpha = 0.8$ (which is lower as compared to the DFA exponent $\alpha = 1.0$ of the healthy subject).

In conclusion, our analysis shows that DFA is a suitable method to quantify correlations in human actigraphy data, independent of the level of overall activity. Unfortunately, our data base of 2 healthy and 2 TBI patients is not sufficient to address our hypothesis and to show a significant difference in the DFA exponents between these two groups. More data need to be recorded, which will be done during the next months, however, it is beyond the time frame of this program. Additionally, the TBI patients will be measured again after undergoing a extensive rehabilitation program at Sheba Medical Center, and our research could be applied to quantitatively evaluate and assess the benefits of such rehabilitation therapy. Moreover, it may be suitable also for other patients who experience difficulties in controlling their limbs, such as after stroke or in patients with muscle spasms.

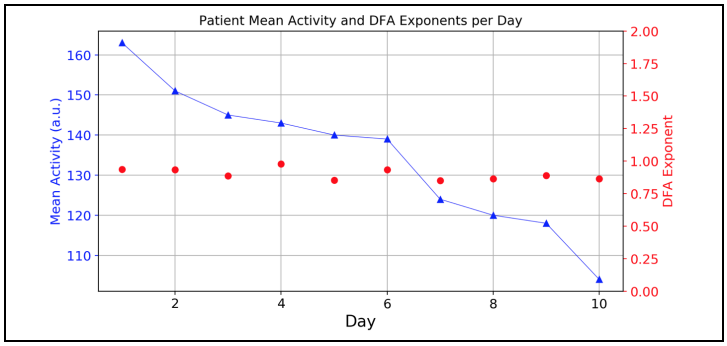

Figure 2: Mean wrist actigraphy data for TBI patient (blue) per day, ordered by activity level (highest to lowest) with DFA exponents of the corresponding days (red). The correlation properties remain constant regardless of activity level.

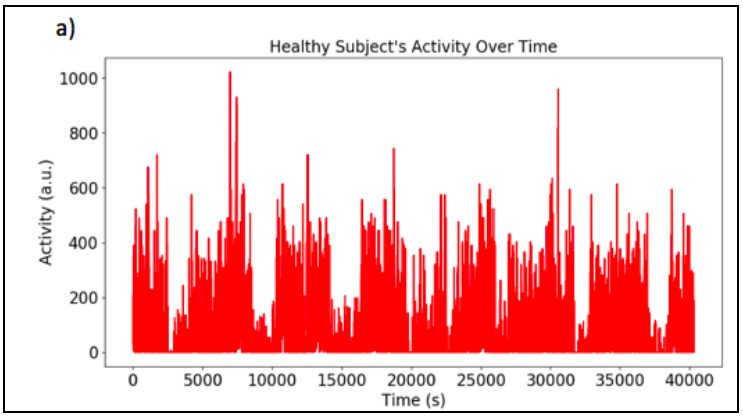

(a)

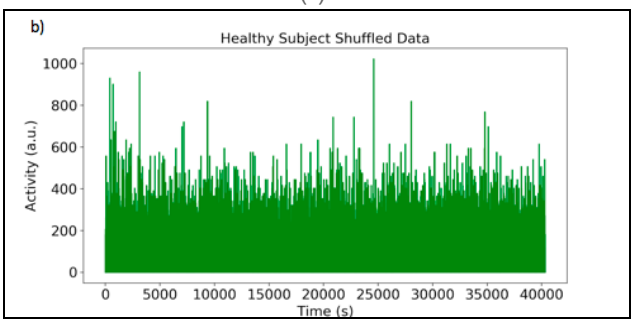

(b)

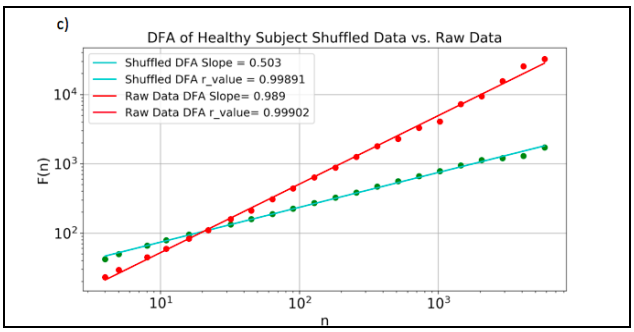

(c)

Figure 1: Wrist actigraphy data for one healthy subject recorded over 7 days and DFA analysis. The raw data for 7 consecutive days are shown in Fig. 1a. Note the patterns of high activity during light periods, alternating with patterns of low activity during the nights. Applying DFA on the raw data yields an exponent of 1.0 (red curve in Fig. 1c). After shuffling the raw data of Fig. 1a, activity patterns and correlation properties are lost (Fig. 1b) and data show characteristics of white noise with DFA exponent of 0.5 (green curve in Fig.1c).

Wannier Functions of Iron-Based Superconductors

Joseph Rubin
Advised under Dr. Emanuele Dalla Torre

Superconductors, when cooled below critical temperature, conduct electricity with virtually no resistance. Understanding their electron orbitals will facilitate creating super-conductors that are economically viable.

The lab of Professor Jennifer Hoffman of Harvard University[5] sent us a 2-D array of scanning tunneling microscope measurements of the conductance, $\frac{\partial i}{\partial v}$, of the conduction band of Iron Selenide (FeSe). Via MATLAB[6] I applied a 2-D Fast Fourier Transform to the conductance for -24 V. This Fourier Transform will henceforth be called a G-map. The phase seems random (Figure 1a).

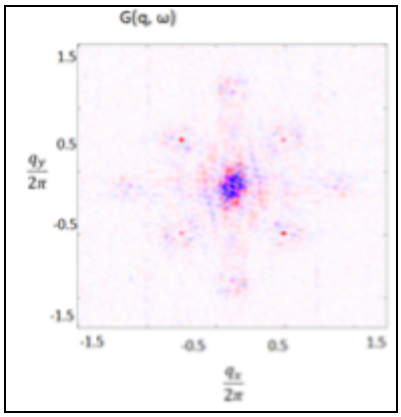

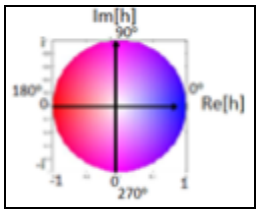

Figure 1a (left): G-Map of FeSe; refer to figure 1b.

Figure 1b (top): HSV represent of complex numbers.

Following Professor Dalla Torre and his colleagues[7], I created holographic maps (h-maps) which are free of phase changes from impurities that randomize the phase of the G-map.

H-maps were made by shifting the G-map by different reciprocal lattice vectors (Figure 2a) and multiplying the G-map by the conjugate of the shifted G-map (Figure 2b).

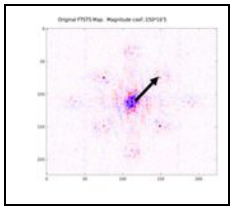

Figure 2a: Example of Reciprocal Lattice Vector.

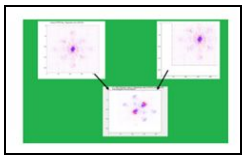

Figure 2b: Multiplication of G-map (top-left) by complex conjugate of shifted G-map (top right).

Eight h-maps correspond to eight reciprocal lattice vectors (Figure 3).

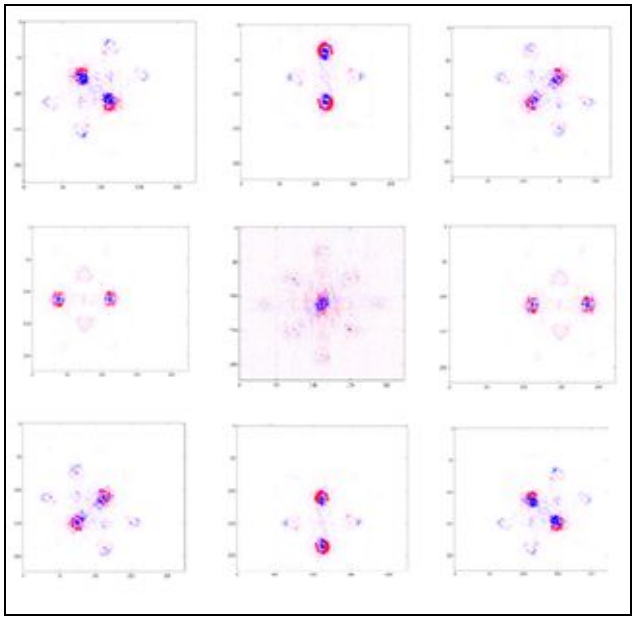

[5] J. Hoffman, STM measurements of FeSe grown on STO12.
[6] MATLAB & Simulink student version (Version R2017b) [Computer software]. (n.d.).
[7] Dalla Torre, E., He, Y., & Demler E. Holographic maps of quasiparticle interference. *Nature Phys.* **12,** 1052-1056 (2016).

Figure 3: Experimental h-maps of FeSe. Center: G-map (figure 1a). Surrounding: h-maps from different reciprocal lattice vectors.

From these, we constructed a g-map with the random phase changes factored out which contains linear sets of zeros that cut across 2-dimensions. (Figure 4).

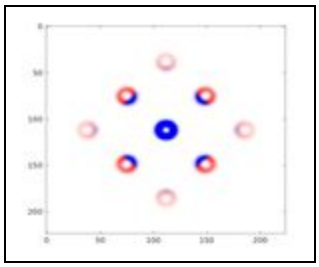

Figure 4: Reconstructed G-Map.

We later constructed theoretical h-maps based on the expectation values of G-maps.

The wave function of electrons in FeSe in real space is a convolution of a Wannier function and a function associated with impurities in the super-conductor (eq. 1).

$$\Psi = W(x,y) \ast F(x,y) \qquad (1)$$

The expectation value is:

$$\Psi^*\Psi = \{W(x,y) \ast F(x,y)\}^* * \{W(x,y) \ast F(x,y)\} \qquad (2)$$

The Fourier Transform of eq. 2 becomes

$$G(q_x,q_y) = \{W^*(q_x,q_y)F^*(q_x,q_y)\} \ast \{W(q_x,q_y)F(q_x,q_y)\} \qquad (3)$$

For $F(q_x,q_y)$, we defined:

$$F(q_x,q_y) = \frac{1}{\eta^2 + \left(\cos(q_x+q_y) + \cos(q_x-q_y) - C\right)^2} \qquad (4)$$

η and C are adjustable constants.

We considered three trial Wannier functions, one with s-wave symmetry (Figure 5a, eq. 5), one with p-wave symmetry (Figure 6a, eq. 6), and one with d-wave symmetry (Figure 7a, eq. 7).

S-Wave function: $w(x,y) = e^{\frac{-(x^2+y^2)}{14.58}}$ (5)

P-Wave function: $w(x,y) = x * e^{\frac{-(x^2+y^2)}{14.58}}$ (6)

D-Wave function: $w(x,y) = (x^2-y^2) * e^{\frac{-(x^2+y^2)}{14.58}}$ (7)

The s-wave (Figure 5a) and p-wave (Figure 6a) do not match the experiment. The experimental reconstructed G-map (Figure 4) has sign changes across 2-dimensions. The s-wave G-map (Figure 5b) has no sign change; the p-wave G-map (Figure 6b) changes sign across only one dimension.

Only the d-wave theoretical g-map (Figure 7b) contains sign changes across two dimensions. We thus concluded the Wannier function of the conduction band of FeSe has d-wave symmetry.

Figure 5: Wannier Function (a) S-Wave G-Map (b) Theoretical G-map based on S-Wave

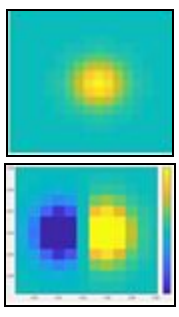

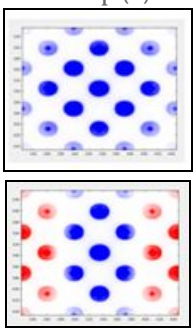

Figure 6: P-Wave function Theoretical G-map based on P-Wave

Figure 7: 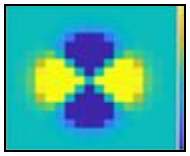 D-Wave Function 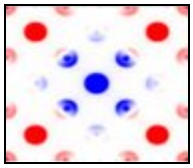 Theoretical G-map based on D-Wave

Brain Science

(L-R) Tzipora Weinberger, Anna Schuman, Nurit Esral, Talia Schiff, Chiya Abramowitz, Elen-Sarrah Dolgopolskaia, Moreet Levine

Using MEG to Analyze Brain Activity Correlated with Counting and Number Recognition

Tzipora Weinberger
Advised under Prof. Mina Teicher and PhD students Ahmad Soleman and Amir Kleks

MEG (Magnetoencephalography) is a non-invasive neurophysiological technique that measures electromagnetic fields of the neuronal activity in the brain. Unlike other brain imaging devices such as the fMRI, PET and SPECT, the MEG has high temporal and spatial resolution, time scales in order of milliseconds and can directly measure brain function. Because of these differences, the MEG is able to clearly examine specific areas of the brain. Neurons on a cellular level have electrochemical properties that produce an outflow of charged ions. The net effect of this ionic current flow creates an electromagnetic field. However, there needs to be somewhere between fifty thousand to one hundred thousand excited neurons for the electromagnetic field to even produce a weak signal. Thus, the MEG machine needs superconducting sensors SQUID (superconducting quantum interference device) so

that data can be collected. The SQUID sensors are immersed in a liquid helium cooling unit. Because of this temperature, impedance is low and the SQUID device can amplify magnetic fields created by neurons a few centimeters away from the sensors.

Earlier fMRI studies have demonstrated that there is no distinction in the brain when individuals see numbers in word or digit form. However, we are trying to pinpoint the part of the brain people use to count in small increments (from two to five). To do this, the participant is placed in the MEG machine and answers questions relating to numbers and counting. The screen first shows the participant two to five circles and they are asked to type how many there are. There is then a 0.7 break before the process starts again. In the next part the colors red blue and yellow are each assigned to a number. The participant is then shown a colored circle and has to indicate the number that correlates to the color. Both of these parts are repeated fifty times. In the final part the participant is shown a number from two to five and they have to indicate the digit. Because this is a part of the control it is done only ten times. The goal of this experiment is to analyze which sections of the brain light up when people see a digit as opposed to counting the number of objects. We predict that the participant's sensory/visual/ auditory area of the brain will react first and then the IPS (Intraparietal Sulcus) will be stimulated. Using PCA (Principal Component Analysis), we will analyze the data we got from the MEG machine to evaluate if this is true. While right now we are only trying to create a distinction between digits and counting, the ultimate goal of this is to find and differentiate the sections of the brain that people use to compute algebra and geometry questions.

The Impact of Semantics and Exposure on Facial Recognition

Elen-Sarrah Dolgopolskaia
Talia Schiff
Advised under Dr. David Anaki

Facial memory is the process by which faces are encoded and retrieved in association with various portions of the brain including the Fusiform Face Area and other important areas in the temporal lobe. In analyzing the processes behind facial memory, we looked at the influence of factors like frequency of exposure to faces and the presence of semantic information, such as a given name or profession. Participants were recruited for a study consisting of four days of daily study and tests of 32 faces per day, varying in frequency of exposure (e.g., 0, 2, 4 times) and accompanying semantic information (e.g. Mike, Verizon Employee). The test asked participants to determine whether a given face was accompanied by semantic information and, if so, to identify it. The fifth day of the study consisted of a review of the 128 faces in preparation for the sixth day's final test, which looked at the additional variable of participants' ability to distinguish between previously and newly presented faces. During this final test, participants were evaluated both behaviorally, on performance accuracy, and electrophysiologically, through the use of event-related potential (ERP), consisting of electrodes in 72 locations across the scalp and face to provide a comprehensive picture of the electrophysiological activity occurring in the brain throughout the test. Another version of the experiment utilized fMRI imaging for the final test.

The behavioral results of the daily tests, as shown in Figures 1 and 2, demonstrated that increased exposure to faces made no difference in participants' recognition of faces when no semantic information was provided. However, when faces were accompanied by semantics, those faces exposed four times yielded better recognition,

showing an interaction effect between the two independent variables. The lack of difference in recognition between the exposure conditions when semantics were not provided can be explained by the lesser challenge in simply remembering that no additional information was given. However, increased exposure did prove to be beneficial for the higher difficulty task of recognizing the faces with semantic information.

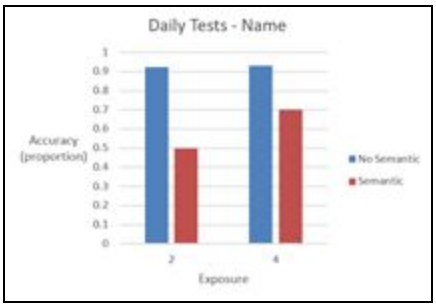

Figure 1

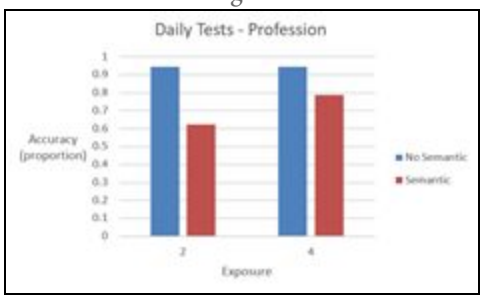

Figure 2

The final test, as shown in Figure 3, looked not only at semantics and exposure, but also participants' ability to identify faces as previously learned or as new. The behavioral results showed trends similar to those of the daily tests for identifying semantics, however, accuracy identifying faces as old or new was higher for those which had originally been presented with semantics. Thus, although memory of the semantic information itself was not of high resolution, its attachment to faces during learning increased participants' familiarity with the faces, allowing them to identify those old faces with semantics with higher accuracy than those old faces without.

The behavioral data of the old/new question on the final test showed two main effects but no interaction effect, meaning both semantics and increased exposure increased recognition but increased exposure did not impact the influence of semantic information, and vice versa. This implies that both semantics and exposure affect face recognition, but based on different processes.

Using Brain Analyzer 2.0 software, performance on the final test was also analyzed through the use of ERP, which recorded all electrophysiological activity as it occurred. Figure 4 shows the cleaned and segmented data from the P10 electrode averaged across the four conditions and 16 participants. The zero millisecond mark corresponds to the presentation of the picture, with the extreme negative dip at 170 milliseconds consistent with the brain wave pattern known to reflect the neural processing of faces, called the N170. The N170 of the four exposures with semantics showed stronger amplitudes than the other three conditions, showing two main effects with an interaction.

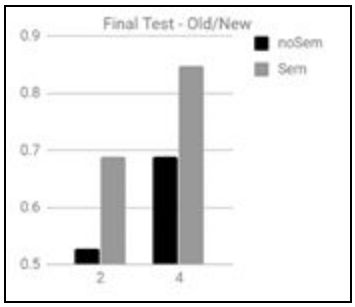

Figure 3

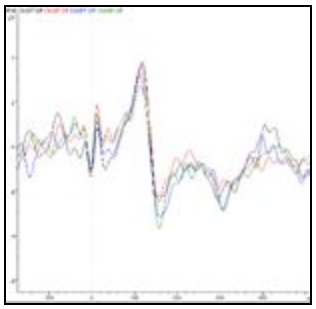

Figure 4

These results have important ramifications for understanding and improving memory. For example, increased age is known to be associated with a decrease in facial recollection, yet not in familiarity (i.e., remembering faces but not names). By understanding these two processes as distinct, it appears that attaching semantic information, such as name and personal details, to new faces benefits familiarity with faces even if not recollection of the names themselves.

Linguistic Analyses of Narratives and Children's Pre-Literacy Skills

Nurit Esral
Moreet Levine
Anna Schuman
Under Prof. Sharon Armon-Lotem and Dr. Carmit Altman

Language, the building block of communication, can be affected by socio-cultural influences, developmental disorders, and acquired conditions. Clinicians use various methods to evaluate speech in order to determine if their clients have language difficulties. This research conducted in the linguistically diverse population of Israel and in America focuses on various testing methods that are used to assess different aspects of language.

In the first study, clinical language assessments collected over the past 15 years in Israel from English-Hebrew bilingual preschool children were examined to study whether socio-cultural differences among religious bilingual Israelis affect their CELF (Clinical Evaluation of Language Fundamentals) test results. The CELF test is a pre-literacy test designed for English-speaking Americans. It assesses a child's language and communication skills and tests their receptive and expressive language abilities. Since the test is based off of American cultural norms it does not account for socio-cultural differences and does not guarantee an accurate description of Israeli children's pre-literacy skills. For example, in one section of the test, the child is shown a picture of a trophy and has to name the item. In the data that was analyzed from the bilingual English-Hebrew speaking participants, many referred to the picture of a trophy as a "gvi'a", which is a goblet in Hebrew. This is an item that is used in many religious homes on the Sabbath and is therefore more culturally familiar to many religious bilingual Israeli children than a trophy. Due to this cultural discrepancy, children who are unfamiliar with the word "trophy" will receive a zero on that test item, but that is not indicative of their pre-literacy abilities. It is therefore crucial for clinicians to be cognizant of socio-cultural influences that can manifest themselves in certain test items and to be cautious not to diagnose a bilingual child exclusively based on test scores.

In the second study, data was analyzed for a pilot project on Narrative Response to Intervention (NRTI) among children with and without a Developmental Language Disorder (DLD). The goal of this study is to see whether NRTI positively impacts the complexity of children's narratives. Their story-telling abilities were monitored four different times throughout intervention. At each of the four monitoring sessions the children used pictures to retell a different story that the interviewer delivered. Hundreds of recordings were transcribed into the CLAN computer program using CHAT (Codes for Human Analysis of Transcripts) conventions. The narratives were then analyzed using a multi-faceted coding system encompassing the macro (story grammar elements) and micro (Mental State Terms and language complexity) structure of the children's narratives. Growth in the macro and micro structure of each participant's narrative can indicate the effectiveness of the treatment.

For the final study, narratives from American adults with and without aphasia were divided into utterances and coded for various elements of language complexity such as grammar, and local and global coherence. Once they are all coded, the results will be analyzed and compared to determine if the disfluencies are typical discourse errors or are qualities of aphasic speech. For instance, several self-corrections within a narrative may or may not be a symptom of aphasic speech. These studies, that are still ongoing, are important to clinicians in their evaluations and diagnoses of individuals with language difficulties. Accurate diagnostic testing and treatment is crucial to the wellbeing of each individual.

Ear Bias of Auditory Selective Attention in Spatial Auditory Processing during Behavioral Dichotic Listening Tasks

Chiya Abramowitz
Advised under Dr. Elana Zion-Golumbic, Paz Har-Shai and Nadav Stoppelman

During multi-speaker conversations, while a given speaker may understand what he or she is trying to convey, the listener may not. This phenomenon of the brain's ability to selectively focus auditory attention on a particular stimulus while filtering out other stimuli, or the cocktail-party effect, has been studied in Dr. Golumbic's lab. The experiments are conducted in dichotic-listening environments; selective attention and speech-sound perception are tested by presenting differing stimuli in each ear.

MEG data for brain lateralization in an experiment on auditory perception of unintelligible speech portrayed a right-hemisphere dominance, which led to the possibility of a left-ear advantage due to contralateral pathway control of the right hemisphere. This was inconsistent with Kimura's structural REA theory model, which is associated with left-hemispheric specialization for language processing during DL-tasks due to structural brain asymmetries and suppressed ipsilateral pathways. However, factors such as age, linguistic complexity, selective attention, memory, language-specific processing, neuromaturation, volume thresholds, alpha-power and beta-activity trends, hand-dominance, and sound-to-noise ratio, were all found to change one's REA preference. It was found that semantically-related words and lower-pitched stimuli presented to the left ear could influence the recognition of an attended word from the right ear, and that those aged 9-59 express a smaller presence of REA. Auditory speech stimuli consisting of syllables and languages with unvoiced words (e.g ba/ka/ta) were also found to elicit a more atypical REA or LEA. Various studies also pointed to new brain pathways models involved during DL-tasks, including the neglect model and the notion that LEA is not always associated with right hemisphere dominance.

A spatial version of the behavioral auditory perception and attention experiment was then conducted to precisely measure the differences between the perception of speech stimuli in the right and left ears. It was set up with the addition of selective speech stimuli presented in spatial-azimuths, or angles at which the auditory stimuli are perceived. The *.wav files in spatial azimuths were coded in MATLAB using HRTF, in a horizontal plane with the selected azimuths of 40°/160°/200°/320°, with 90° representing the right ear, 180° as back of head, 270° for left ear, and

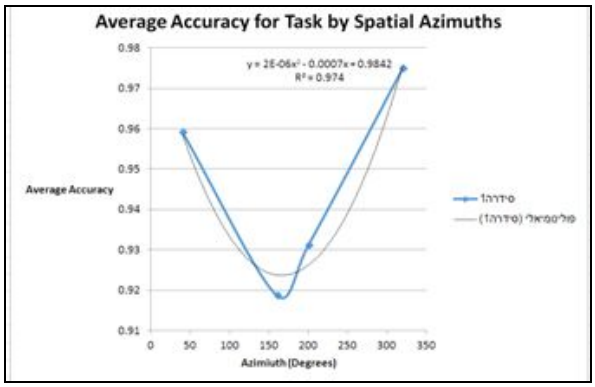

Figure 1

360°/0° for front of head. Each participant entered a soundproof room and heard a series of auditory stimuli consisting of various Hebrew words presented at 4 Hz through headphones, and reported how many times the word 'etz' was repeated. Sometimes the participant would selectively listen to how many times one of the speakers would say 'etz', and sometimes would listen to how many times all of speakers said 'etz'. The experiment consisted of 144 questions with

equal amounts of male/female voices, two/four speakers, and selective/divided tasks.

The results yielded a positive parabolic function for accuracy by increasing azimuth angle of each 3D-sound stimulus, with the 40° and 320° azimuths yielding the highest accuracy and the 160° and 200° azimuths yielding the lowest accuracy. The highest accuracy levels found near the front of the head, and the lowest accuracy levels were found at the posterior side around the 180° azimuth (Figure 1). The average accuracy at each azimuth was significantly higher for the 2-speaker condition, especially for the 180° azimuth. The participants had difficulty with the selective task and the 4-speaker condition. The spatial experiment contained higher accuracy levels than the earlier non-spatial experiment, but a large difference was observed between the selective accuracies. The spatial data depicted a sharp decrease in accuracy for the selective 4-speaker condition, due to the difficulty in paying attention to one speaker while filtering out the three others in a spatial DL-environment (Figure 2). Moreover, a decreasing trend in accuracy was found over the course of the experiment due to a decrease in attention level. Even though there was an increase in accuracy over time for the higher-variance divided task, there was an overall decrease in accuracy from the start of the experiment at 0.920 to the end at 0.875, decreasing by 4.5%, with a fluctuating function in accuracy throughout.

Although the experimental results may seem convincing, high standard errors, variances, and p-values for the important datasets, program bugs, experimental weariness, and deleted results may have led to statistically insignificant and inconclusive results. However, before analyzing the significance of spatial auditory perception with brain activity in future experiments involving MEG or fMRI procedures, it is important to understand the underlying ramifications for understanding spatial selective auditory perception and attention in the cocktail-party effect through basic behavioral experiments.

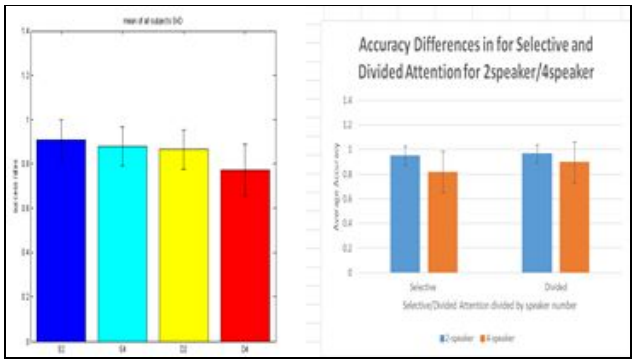

Figure 2